1976-05

Island Barrier Effects on Sea State as Revealed by a Numerical Wave Model and DMSP Satellite Data

Fett, Robert W.; Rabe, Kevin M.

Journal of Physical Oceanography, Volume 6, pp. 324-334
https://hdl.handle.net/10945/45769

Island Barrier Effects on Sea State as Revealed by a Numerical Wave Model and DMSP Satellite Data

ROBERT W. FETT AND KEVIN M. RABE

Environmental Prediction Research Facility, Naval Postgraduate School, Monterey, Calif. 93940

(Manuscript received 17 September 1975, in revised form 26 January 1976)

ABSTRACT

Island barrier effects on the state of the sea in the lee of islands have been studied by means of a numerical wave prediction model and by examination of data from sensors of the Defense Meteorological Satellite Program (DMSP), the Synchronous Meteorological Satellite (SMS), and the Earth Resources Technology Satellite (ERTS). Visual indications of calm areas in the lee of the Lesser Antilles, evidenced by a marked reduction in the satellite-observed sunglint at selected sun angles, are verified by the results from the numerical wave model; other lee reflective patterns correspond to areas of changed sea state. These results indicate that a reduction in the swell height, alteration of the period, and reorientation of the swell direction, in many instances long distances to the island's lee, are responsible for the satellite-observed reflective patterns noted. The additional phenomena of bow waves and wind-induced oceanographic eddies are also examined, and some evidence of their occurrence and detection is presented.

1. Introduction

Several recent studies have investigated lee island effects in relation to wave refraction and atmospheric blocking by island topography. Patzert (1969), examining the tradewind flow around Hawaii, noted a distinct wind minimum in the lee of the islands, with consistently stronger winds to be found in the intervening channels. The channel flow was interpreted to be analogous to Venturi flow through a constricted opening. Some visual verification was obtained from the Gemini-9 flight on 6 June 1966 over the Canary Islands area (NASA, 1968). Photographs revealed a distinct dark area extending a short distance to the lee of several islands, in areas which were otherwise sharply illuminated by sunglint. The dark areas were attributed to the sheltering influence of the islands on atmospheric flow, which resulted in calm seas to the lee. Stevenson *et al.* (1970), in a review of Apollo-9 photographs, noted similar features. It was theorized that the effect was a turbulent oceanographic feature or wake resulting from wave refraction around the island, the wake being one of a series, continuously forming and shedding off from the island. Stevenson (1970) later contended that this series extended in a broken pattern at least 222 km downstream. Barkley (1972) presented further evidence that a current flow of sufficient velocity produces a lee wake of cyclonic eddies, in studies performed in the lee of Johnston Atoll.

Cram and Hanson (1974) unsuccessfully attempted to relate ERTS-1 photographic features to eddy formation in the Antilles. They concluded that the features observed resulted from horizontal differences in the sea-surface roughness due to a wind-shadow effect exerted by the island topography. Using NOAA-2 data (Fig. 1) Strong *et al.* (1974) also studied the reflectance patterns of the Lesser Antilles and came to much the same conclusions. The reflectance patterns were assumed to be relatively calm areas, with heights of less than 0.5 m for wind speeds of approximately 5 m s^{-1}. The patterns were found to extend downwind almost 200 km.

2. Geometrical aspects of DMSP sunglint relationships

Sunglint patterns are apparent in most daytime DMSP passes. An example of a typical sunglint pattern obtained in a direct readout at San Diego, Calif., is shown in Fig. 2. The sunglint pattern forms a band from the bottom to the top of the central portion of the figure, with the dashed subsatellite track nearly bisecting the pattern into two symmetrical halves.

This pattern is much different from the nearly circular sunglint pattern observed by geostationary satellites. The reason for the DMSP pattern can be understood by reference to Fig. 3. As the spacecraft progresses northward at an altitude of 833 km (450 n mi) from point A to point D, points of possible specular reflection (where zero or horizontal slope reflection occurs) are located along great circle arcs connecting the subsatellite point with the subsolar point. The approximate distance to any point X can be calculated by applying the nomogram in Fig. 4. However, the satellite is

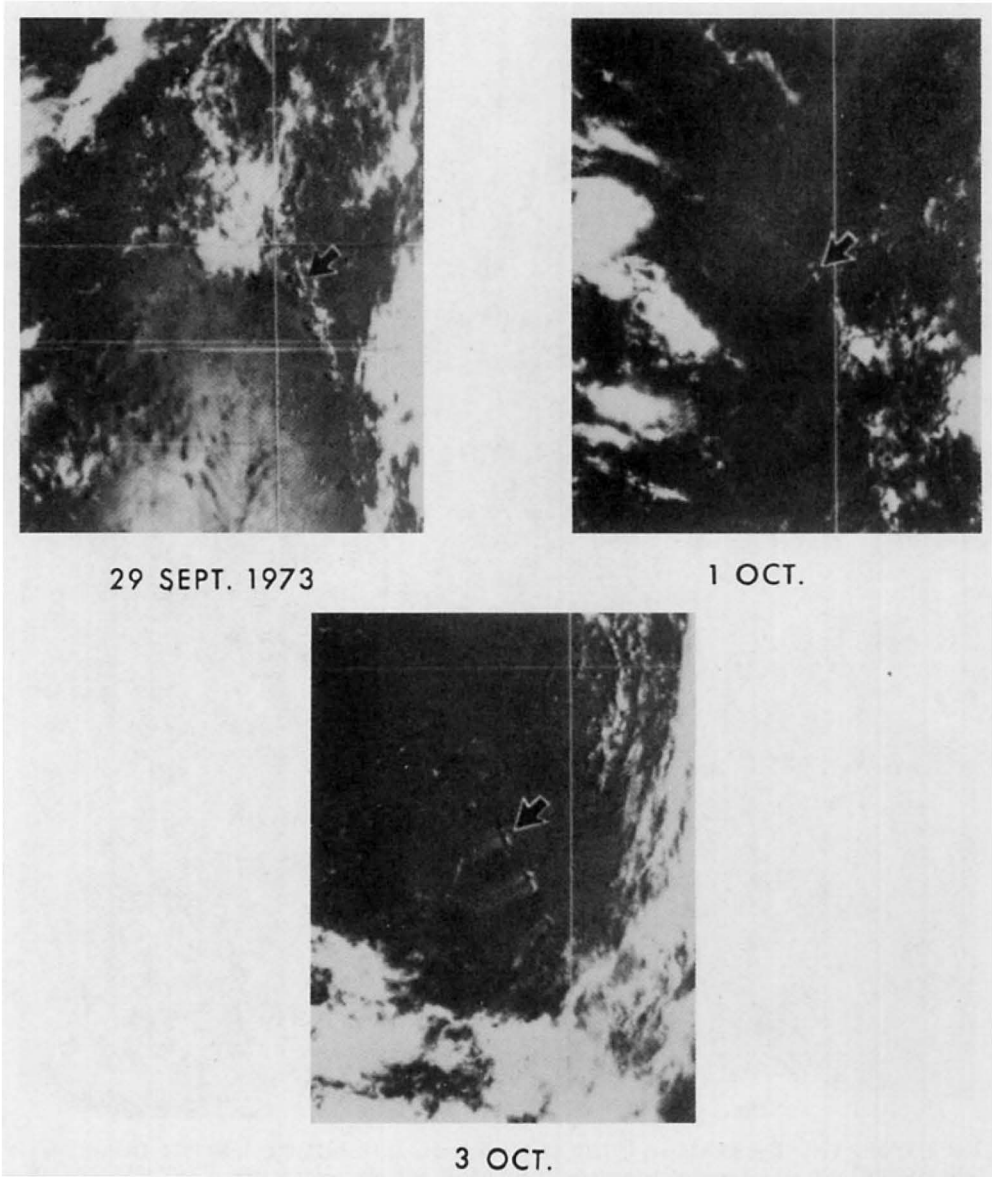

FIG. 1. Very High Resolution Radiometer (VHRR) images of the Lesser Antilles. (White north-south synchronization line is embedded in the image.) Guadeloupe Island is located by arrows (from Strong *et al.*, 1974).

capable of detecting specular reflection only at point B, since the scanning radiometer sweeps from horizon to horizon, perpendicular to the subsatellite track. Sunglint detected at other points such as A and C is nonspecular, and possible only because of diffuse reflection off a disturbed sea that has wave fronts appropriately oriented to provide the required geometry. Sunglint continues to be detected with steadily decreasing intensity beyond point C until arrival near point D, where the scanner is no longer capable of viewing any portion of the sunglint area. Maximum reflectivity is normally sensed along the curve connecting all points of possible specular reflection. This accounts for the pattern shown in Fig. 2, including the displacement of the band from the subsatellite track. Sea state and atmospheric conditions can act to modify this pattern such that sunglint effects may not be detected or if detected, appear asymetrical or offset from the anticipated pattern.

Fig. 5 is a DMSP pass over the western Pacific in which brilliant specular reflection is observed near 30°N. This brilliant specular reflection is the result of a relatively calm sea state. The anomalous dark areas to either side are also interpreted to be calm, as discussed by Parmenter (1969) and McClain and Strong (1969).

Fig. 6 gives a theoretical sea-surface sunglint composite pattern which relates to this example. The dark swath represents calm conditions in an otherwise uni-

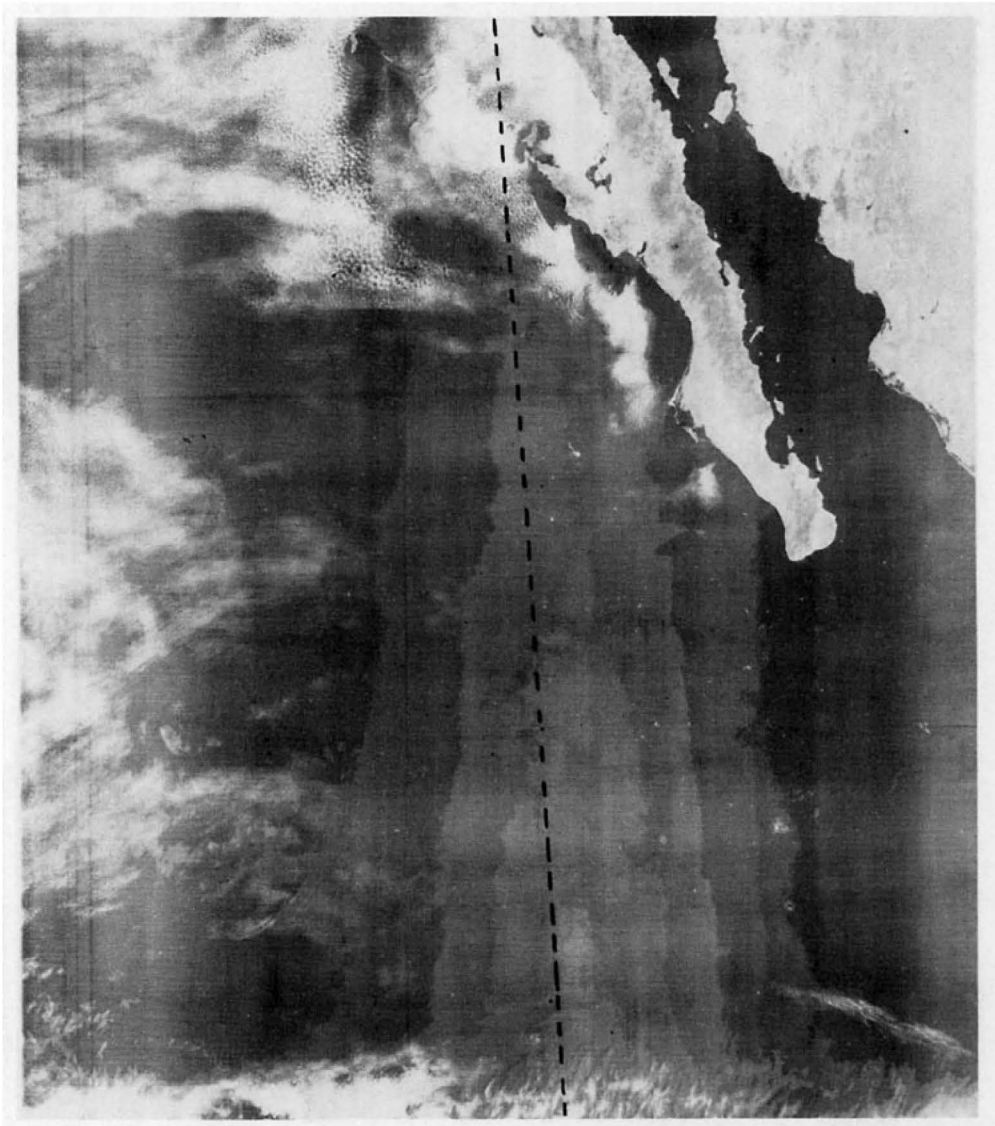

FIG. 2. DMSP Very High Resolution (VHR) visible depiction at 1853 GMT 8 April 1974. Dashed line is the satellite track, which crosses the equator at 108.65°W. Subsolar point is located at 7.4°N, 102.6°W.

form wind field of 5 m s^{-1}. A reflectance measurement of 5000 units is indicated at the specular point. Reflectance is reduced drastically east and west of this point in the calm area, resulting in the very dark shades shown in the actual example of Fig. 5. An important implication is that, away from the immediate vicinity of the specular point, calm sea states should appear much darker than the surrounding non-calm seas. It is this relationship that is applied to interpretations of observed reflectance patterns in the following sections.

3. The numerical model

To aid in the interpretation of the DMSP data, it was considered desirable to quantitatively describe the island barrier effects upon sea and swell, produced by varying wind conditions. Since an adequate sample of observations was unavailable, a numerical model was utilized for this aspect of the study; the French spectro-angular wave model (D.S.A. V) was selected because of its spatial growth and decay features and its treatment of angular advection and dispersion (Gelci *et al.*, 1963).

Mathematically, the basic method used by the model can be expressed by the equation

$$d\rho/dt = F[W, |\theta - w|, T] - (A\rho/T^4)m_0 - V_{(T,\theta)}\mathrm{Grad}\rho_{(T,\theta)},$$

where the change in spectral density, $d\rho/dt$, is described by a spectral increase term, a decay term, and an advective term dependent upon the group velocity. The spectral increase term utilizes the components of the wind field as its only driving forces. The wind speed W (m s^{-1}), and the wind azimuth $[\theta - w]$ (w being the wind direction and θ a computational direction)

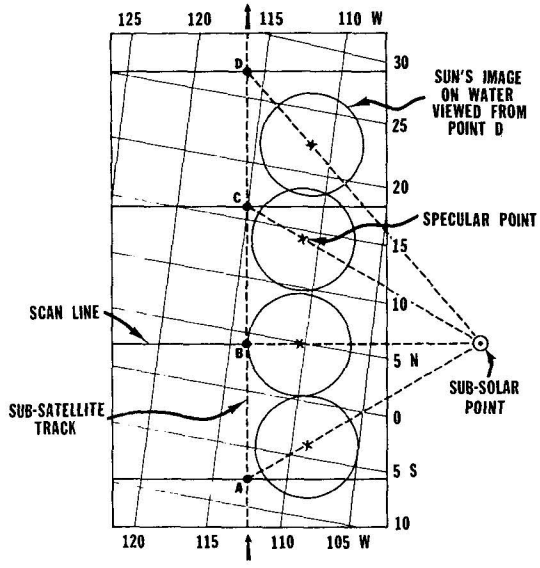

FIG. 3. Schematic illustrating sunglint specular point relationships as a function of changing satellite positions, relative to the subsolar point.

impart energy to the sea state, dependent upon the period T of the sea state present. Decay is accounted for by the interaction of the sea state components m_0 and the empirical dampening coefficient A. The advection term is a function of the gradient of the spectral

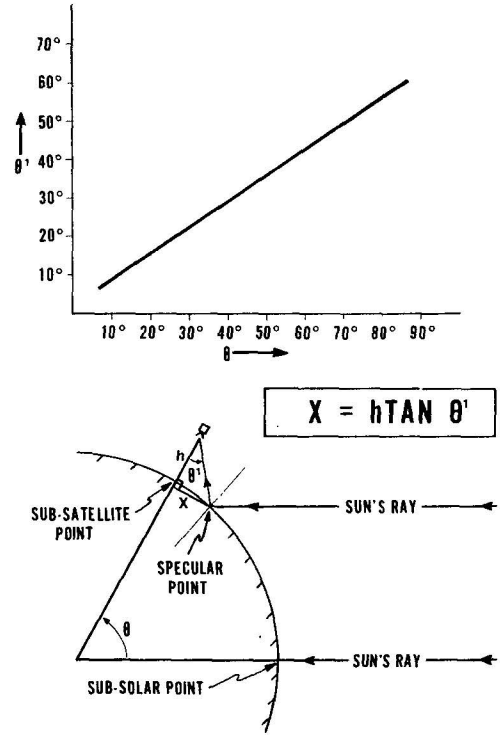

FIG. 4. Schematic and nomogram for computing distance to specular point location from the subsatellite point. The nomogram was developed for a satellite height of 833 km (450 n mi).

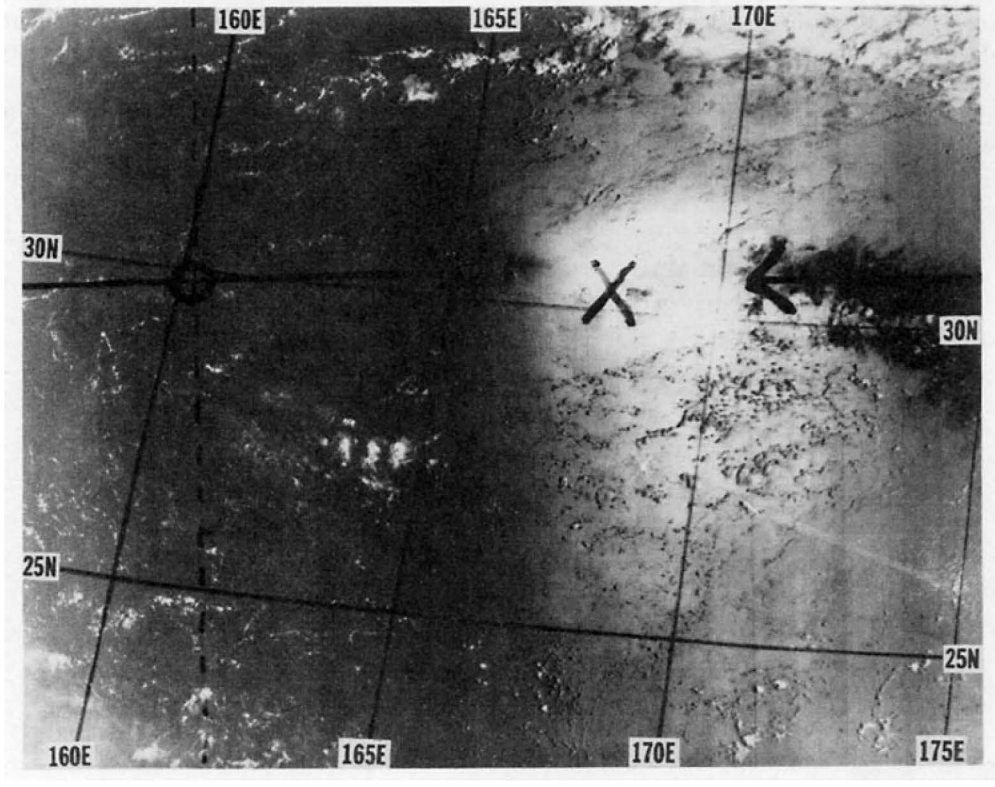

FIG. 5. DMSP VHR visual depiction at 2105 GMT 14 July 1974. The dashed line is the subsatellite track. The circle on the track represents the subsatellite point. The line through the circle represents a scan line. The specular point location is denoted by an ×. The arrow is on the great circle arc connecting the subsolar point, the specular point, and the subsatellite point. Subsolar point location was 21.6°N, 134.8°W.

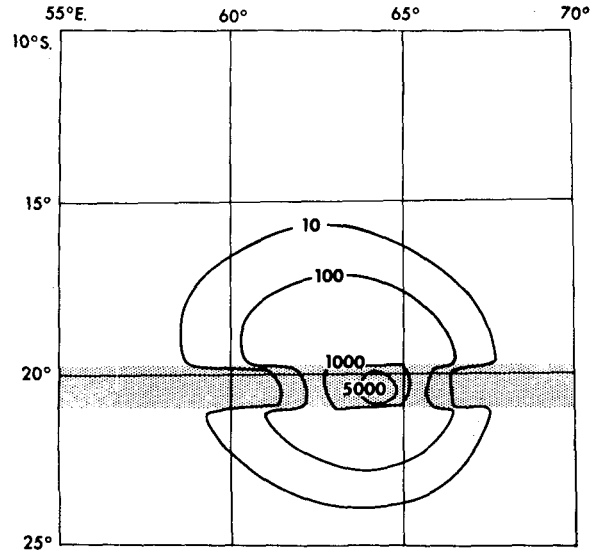

FIG. 6. Theoretical sea-surface sunglint for a composite pattern: 5 m s^{-1} wind background and a calm wind in an east-west swath near specular point (shaded). Isopleths are relative reflected intensity per 10^4 sr incident flux; subsatellite point, 21.5°S, 65.5°E; subsolar point, 5.8°S, 35.6°E; satellite height, 722 km (from McClain and Strong, 1969).

densities between points and the unit speed of a swell packet, $V = gt/4\pi$, where g is the acceleration of gravity.

A grid using a 40 n mi (74 km) grid interval was constructed for the study. A square island with 80 n mi (144 km) sides was introduced in the middle of the grid, and a uniform wind field was assumed to exist at each grid point except in the lee of the island where, for three grid intervals (222 km) downstream, wind speeds were reduced to 2.5 m s^{-1} in all instances. The lee wind reduction was devised to simulate island topographical blocking effects on atmospheric flow. The results of the numerical experiment and their relationship to the satellite-observed effects are discussed in Section 4.

4. Results and observations

a. Island barrier effects on swell height in the lee of islands

If the geometrical reasoning developed in Section 2 is followed, an alternate explanation for the features observed in Fig. 1 is possible. A calculation of specular point location for the data on 29 September 1973 reveals it to be over 300 km west of Guadeloupe at the time the spacecraft was viewing that area. The main zone of specular reflection is well to the southwest of the islands, as can be seen near the bottom of the figure. The islands, therefore, are on the very fringe of the diffuse sunglint area. Accordingly, calm areas or relatively calm areas should appear darker than the surrounding seas and not lighter.

In fact, Strong *et al.* (1974) noted small dark areas in the immediate lee of the islands on the 29 September 1973 depiction (Fig. 1). Under the reasoning presented here, these features should correlate with extremely calm seas. The reflective patterns extending beyond the small dark areas, however, cannot represent calm seas; more reasonably, they result from greater concentrations of diffuse reflection, brought about by a reorientation and change in characteristics of the wave fronts in the lee of the islands.

This conclusion is also suggested by an inspection of results from the numerical model; Fig. 7 shows the resulting $H_{1/10}$ fields for wind speeds of 7.5 and 15 m s^{-1}.

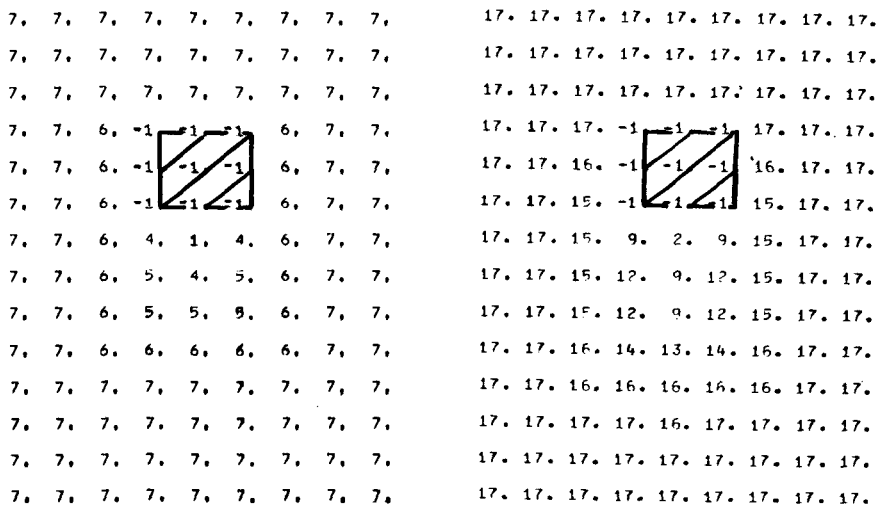

FIG. 7. Numerically simulated sea height depictions (ft) at hour 39 for surface wind speeds of 7.5 and 15 m s^{-1} (2½ m s^{-1} in lee of the island). Sea heights shown are average values for the highest 10% of the swell ($H_{1/10}$); average swell height ($\bar{H}$) is $H_{1/10} \div 2.03$.

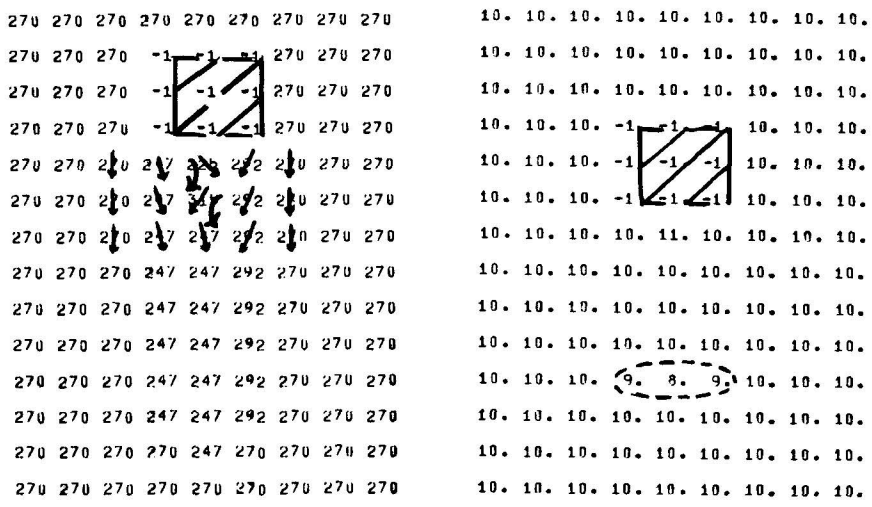

FIG. 8. Numerical simulations of direction of swell around and in the lee of an island at hour 39 under wind speed conditions of 7½ m s^{-1}, and swell period (s) around and in the lee of an island at hour 39 under wind speed conditions of 15 m s^{-1}. Wind is from the west or top of the figure.

A pronounced sea height minimum is evident one grid interval downstream, in the immediate lee of the island, for both wind speeds. A rapid increase in height occurs at surrounding points, though it is still markedly reduced in comparison to the swell of the open sea. Fig. 8 demonstrates how the direction of maximum energy, corresponding to the wave fronts, bends passing by the island, with a corresponding lengthening of the

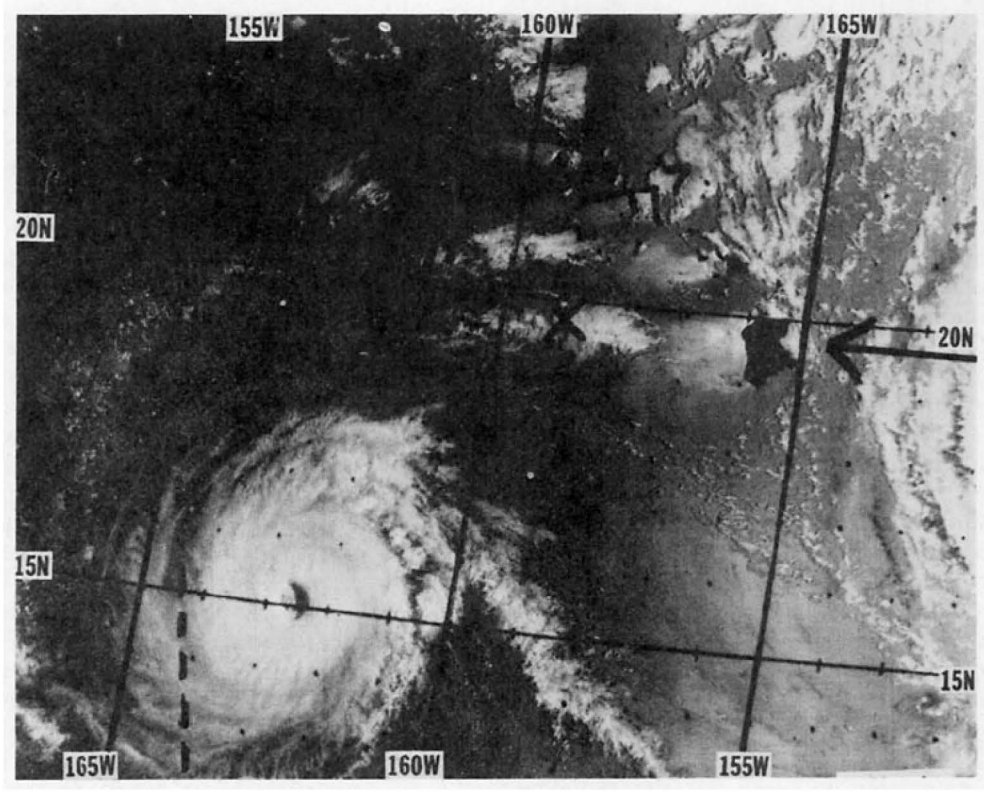

FIG. 9. DMSP VHR visual depiction at 1917 GMT 17 August 1972. Description as in Fig. 5, except wind reports are in knots (1 barb = 10 kt). Subsolar point location was 13.2°N, 108.3°W. Hurricane Celeste, intensity 85 kt, appears SW of the island chain.

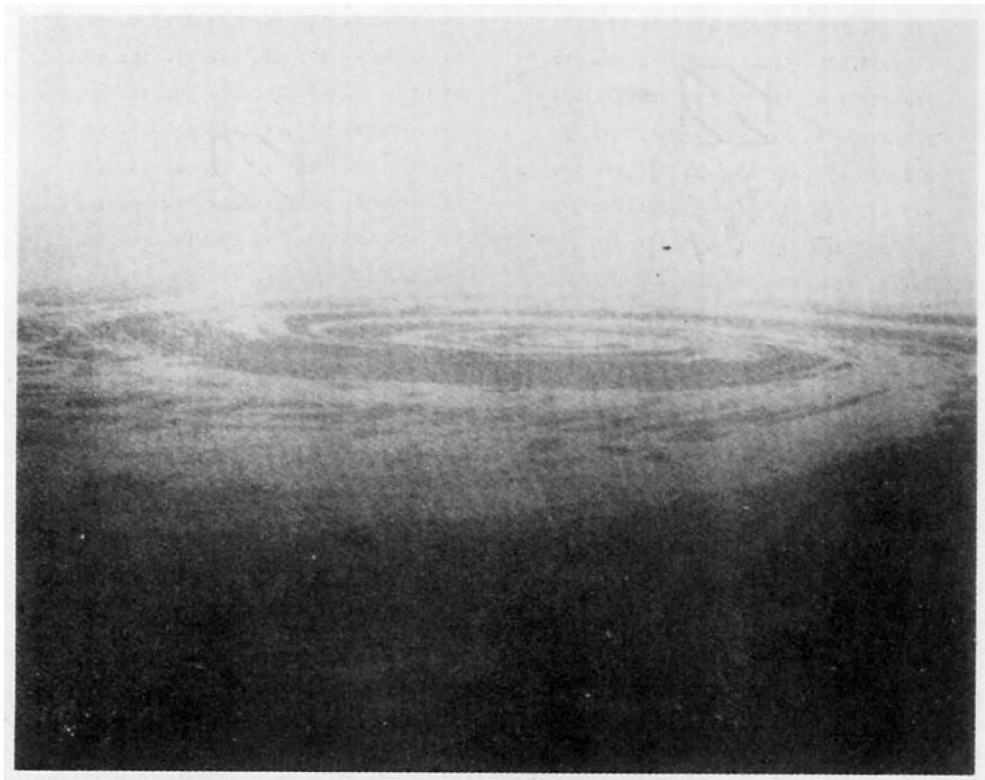

FIG. 10. Sea-surface slicks off San Clemente Island, California, resulting from a large circular eddy circulation of approximately 2 mi in diameter (from LaFond and LaFond, 1971).

period of maximum energy in the immediate lee of the island. The reduced sea height and lengthened period at this point correspond remarkably well with the location of the small, black, presumably calm areas to the lee of the Lesser Antilles (as seen in Fig. 1).

As might be anticipated, wind variations could rapidly disrupt lee refractive patterns and exert an overriding influence on sea state, depending on the strength of the flow. The NOAA-2 view of 3 October 1973 (Fig. 1) is interesting in this respect since the island of Marie Galante (small, dark area just south of the arrow pointing to Guadeloupe Island) exhibits no reflective lee effect. Since the highest point on this island is only 205 m, its ability to restrict airflow to the lee is limited. The refractive wave pattern around the island, therefore, is apparently overridden by the force of the wind so that wave forms in the lee of the island are similar to those in the surrounding area. Similarly, valley areas on the main islands allow the passage of winds which immediately disrupt the lee refractive patterns so that alternate dark swaths are often seen within the reflective areas.

If this interpretation is valid, it must also follow that the reflective areas are areas of reduced wind speed. Thus winds may be relatively calm or lighter in these areas than in the outlying areas; on the other hand, the sea state cannot be calm but could be reduced, as suggested by the numerical model results.

Fig. 9 shows an example of reflective lee effects in the wake of the Hawaiian Islands as viewed by the visual Very High Resolution (VHR) scanner of a DMSP satellite. At the time these data were recorded, the subsolar point was located at 13.2°N and 108.3°W. The Hawaiian chain lies considerably northwest of this location with the specular point indicated by the ×, west of Hilo, Hawaii. The fact that brilliant reflection is not in evidence near this point can most reasonably be attributed to rougher seas in the area. This is the reverse of the more customary interpretation of sunglint patterns near the specular point, when the seas are calm, but is equally valid. As an example, Strong *et al.* (1972) documented a dark streak through brilliant reflection in the Gulf of Tehuantepec, and attributed it to a brisk northeasterly wind diffusing the specular reflection in that area. Note that the plotted wind reports show a rapid acceleration from 7.5 to 15 m s^{-1} over the specular area, which would support a rapid increase in sea height. The ship report in the reflective pattern west of Oahu is especially important since a sea height of 0.9 m was indicated. This observation is consistent with the numerical wave height predictions and is additional verification that the reflective patterns

are not calm as previously thought except in the immediate lee. The reflective patterns can actually represent a quite well developed sea state; this sea state, however, is reduced in comparison to outlying areas.

b. Swell directional changes in the lee of islands suggesting eddy formation

Eddies are commonly found associated with oceanic fronts and continental shelves, and have been noted in the lee of islands; Patzert (1969), Barkley (1972), White (1973) and others have directly observed these features. Fig. 10 shows an eddy in the nature of a surface slick pattern observed downstream of San Clemente Island, California, by LaFond and LaFond (1971), as seen from an aircraft. Viewed from above, the pattern was almost 2 mi in diameter and was related to the subsurface structure of the water column. Fig. 8 appears to show a turbulent lee eddy effect in the numerical wave model results in both the directional and period fields. The directional field has been enhanced somewhat to show the probable circulation pattern. The anomalous low-period area can be construed to be an eddy that has shed off from the island and moved downstream.

Eddies are commonly associated with the mass transport and velocity fields and it should be noted that the numerical model does not directly compute these terms. What results is an implied velocity field based on the distribution of wave energy throughout the spectrum at a given point. A resulting shift in the direction and period of maximum energy can therefore be construed as directly implying a corresponding shift in the wind-driven flow. The results here are somewhat inconclusive, mainly because of the 74 km grid spacing of the model.

Stevenson *et al.* (1970), utilizing pictures from the Apollo-9 spacecraft, hypothesized the general appearance of eddies from space. Fig. 11, a view of the Cape

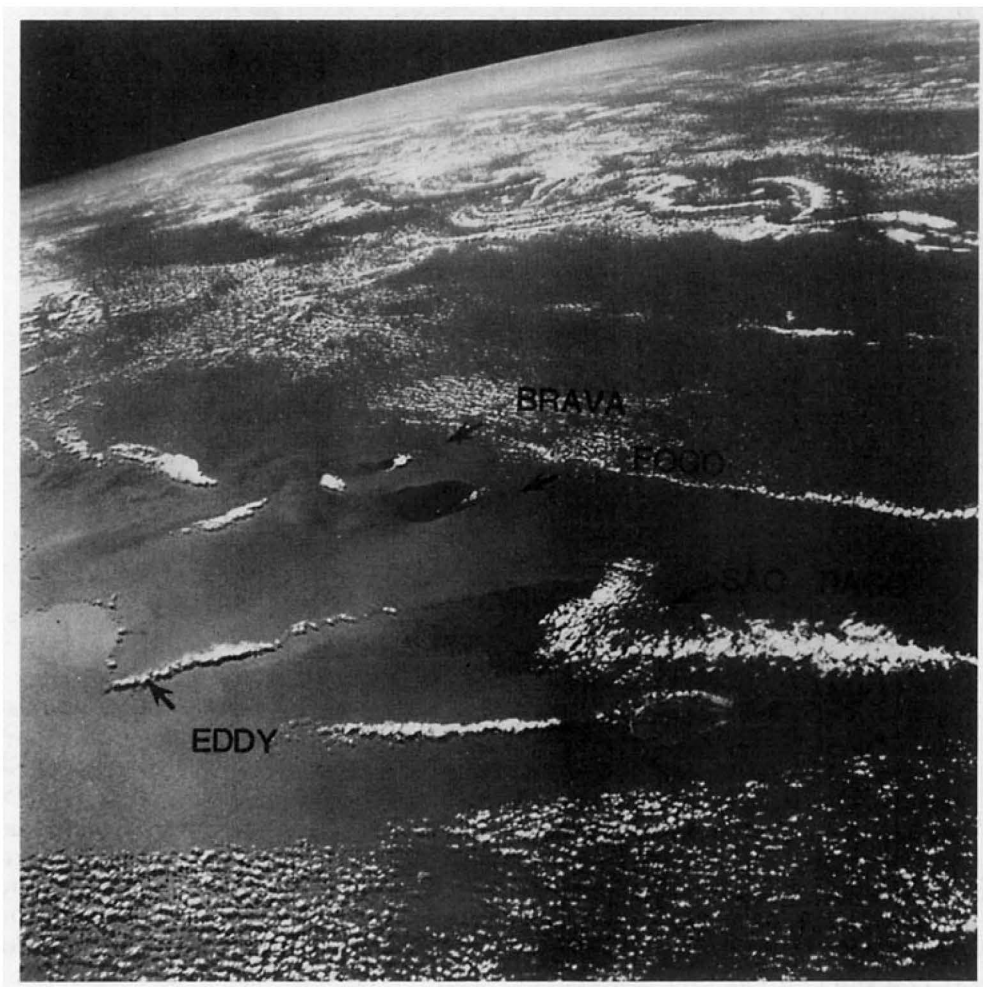

FIG. 11. Visual depiction of the Cape Verde Islands taken from Apollo-9, 9 March 1969, NASA photo number AS9-22-3422 (from Stevenson *et al.*, 1970).

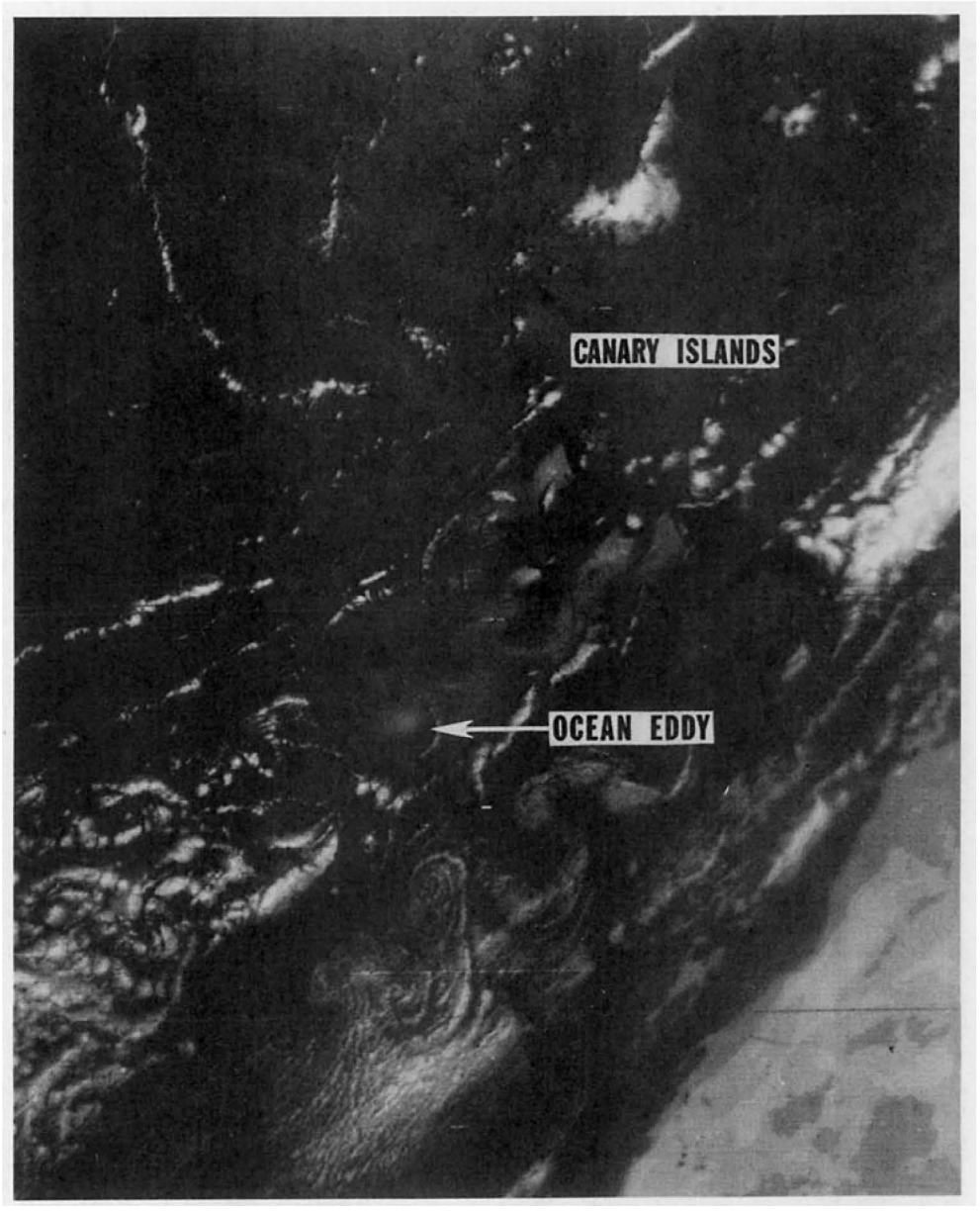

FIG. 12. DMSP VHR visual depiction of the Canary Islands and vicinity at 1022 GMT 10 July 1975.

Verde Islands taken by Apollo-9 on 9 March 1969, demonstrates the distinctive features he noted: the "puff-ball" clouds edging the eddy and the increased reflectance of the interior of the eddy. Later observations of the Yucatan Current from Skylab photographs and the use of airborne expendable bathythermographs confirmed that these were typically cold water eddies (Stevenson, 1974).

Fig. 12 shows a DMSP depiction of the Canary Islands, taken at 1022 GMT 10 July 1975. The pattern of clouds and reflectance which delineates an apparent oceanographic eddy is readily observable downstream of the islands. The infrared data from the DSMP sensor lacks the thermal resolution necessary to determine whether this was actually a cold water eddy. Also, due to the characteristics of the water vapor absorption spectrum in the range sampled by the DMSP sensor, the high reflectance observed could be partially due to a lessening of the water vapor content caused by a lee drying effect in that area. However, it is felt that this possibility would only enhance the reflectance observed and could not, by itself, account for the eddy pattern. This conclusion is supported by independent evidence of oceanographic eddies in ERTS and SMS-2 data which sample portions of the visible spectrum where water vapor absorption is not a significant factor.

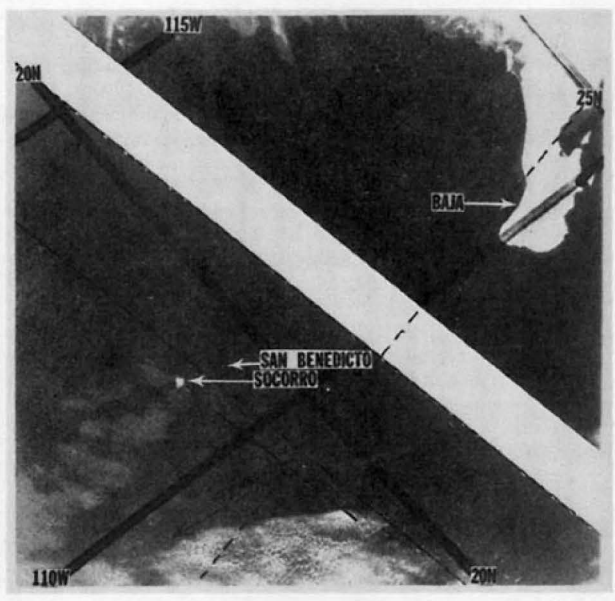

FIG. 13. DMSP VHR visual depiction at 1928 GMT 5 November 1974. Description as in Fig. 5, except specular point is out of picture at 424 km SSW.

c. Apparent bow-wave effect

Using Gemini-10 photographic data, Emery and Stevenson (1972) discussed the possibility of observing bow waves with respect to an island, specifically, Taiwan. The feature results from the flow of an oceanic current past an island, producing an effect similar to that of a ship moving through the water.

Fig. 13 shows a possible bow-wave effect off the island of Socorra, as revealed by DMSP. Surface observations taken in the same time-frame reported clear skies and moderate wind, and a 1.35 m swell approaching from 360°. Therefore, the possibility of these features being the result of cloud formation is highly unlikely. The next logical explanation is that the sensor is observing diffuse sunglint reflected from reoriented wave fronts similar to a bow wave. The specular point was about 3.82° (424 km) southwest, so the area lay on the fringe of the measurable sunglint area.

Fig. 14 shows the results of the numerical model for a wind speed of 7.5 m s^{-1}. A pronounced wake-type pattern to the $H_{1/10}$ field is evident, and the corresponding directional shift to the north and south of the island of 22.5° from the background flow are evidence suggesting the presence of a bow wave. The large grid step prevented detailed inspection of this feature and the possibility remains that this is actually an area of pronounced swell refraction.

5. Summary and conclusions

This analysis has sought to explore more completely the relationship between island barriers and the observed sea state through the use of a numerical wave model and available satellite data. The results indicate that calm seas normally do not extend great distances to the lee of islands, although there is a reduction in swell height which extends far downstream. The calm areas, as well as those disturbed areas of refracted wave fronts, can be detected by satellite sensors. Evidence of eddy formation was found in both the numerical model results and in the satellite data; these data also apparently revealed an island bow-wave effect.

Further detailed investigations are required to document, through additional ground truth, the effects noted in the present analysis. Also to be investigated are the effects of the atmosphere on reflectivity, a factor influencing lee patterns which is readily apparent DMSP data.

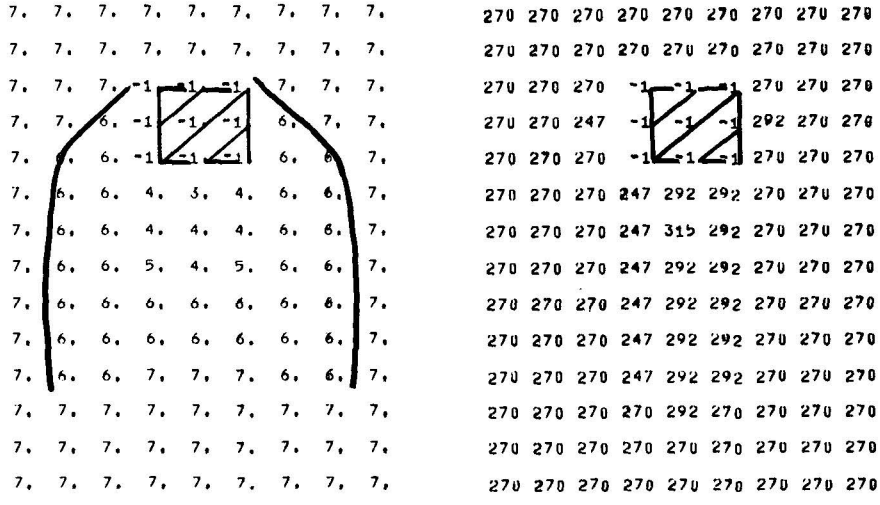

FIG. 14. Numerical simulations of sea height ($H_{1/10}$) and swell direction at hour 15 under wind speed conditions of 7½ m s^{-1}.

REFERENCES

Barkley, R. A., 1972: Johnston Atoll's wake. *J. Marine Res.*, **30**, 201–216

Cram, R., and K. Hanson, 1974: The detection by ERTS-1 of wind-induced ocean surface features in the lee of the Antilles Islands. *J. Phys. Oceanogr.*, **4**, 594–600.

Emery, K. O., and R. E. Stevenson, 1972: Taiwan: A ship at sea. *Acta Oceanogr. Taiw.*, **2**, 1–10.

Gelci, R., P. Chavy and E. Devillaz, 1963: Numerical treatment of the state of the sea. *Cah. Oceanogr.*, **15**, 153–160.

LaFond, E. C., and K. G. LaFond, 1971: Sea-surface slicks. *Proc. NUC Symp. Environmental Preservation*, San Diego, U. S. Naval Undersea Center, 75–103.

McClain, E. P., and A. E. Strong, 1969: On anomalous dark patches in satellite-viewed sunglint areas. *Mon. Wea. Rev.*, **97**, 875–884.

National Aeronautics and Space Administration (NASA), 1968: Earth photographs from Gemini VI through XII. Scientific and Technical Information Division, 327 pp.

Parmenter, F. C., 1969: Picture of the month—Sunglint. *Mon. Wea. Rev.*, **97**, 155–156.

Patzert, W. C., 1969: Eddies in Hawaiian waters. Hawaii Institute of Geophysics, ONR Contract NONR-3748(06), 51 pp.

Stevenson, R. E., 1970: Oceanographic data requirements for the development of an operational satellite system. *Proc. Princeton Univ. Conf. Aerospace Methods for Revealing and Evaluating Earth's Resources*, Princeton, N. J., 12.1–12.12.

——, 1974: Observations of Skylab of mesoscale turbulence in ocean currents. *Nature*, **250**, 638–640.

——, G. Larson and C. L. Kober, 1970: Oceanographic applications of an earth-resource satellite system. *Inter-ocean*, **70**, No. 2, 121–140.

Strong, A. E., R. J. DeRycke and H. G. Stumpf, 1972: Satellite detection of upwelling and cold water eddies. *Proc. 8th Intern. Symp. Remote Sensing of Environment.*, 1069–1081.

——, —— and ——, 1974: Extensive areas of reduced waves leeward of the Lesser Antilles. *J. Geophys. Res. Lett.*, **1**, 47–49.

White, W. B., 1973: An oceanic wake in the equatorial undercurrent downstream from the Galapagos Archipelago. *J. Phys. Oceanogr.*, **3**, 156–168.